Journal of Applied Mechanics and Technical Physics, Vol. 45, No. 3, pp. 311–315, 2004

MAGNETIC DIPOLE MOMENT FROM A ONE-KILOTON UNDERGROUND NUCLEAR EXPLOSION IN A CAVITY

N. G. Karlykhanov, A. A. Kondrat'ev, Yu. I. Matvienko, and V. N. Nogin

UDC 537.8:536

This paper reports the results of numerical modeling of the magnetic dipole moment produced by displacement of the Earth's magnetic field in a one-kiloton underground nuclear explosion in a cavity. It is shown that with increase in cavity size, the magnetic dipole moment increases, reaching 10^7 A · m^2*, which is approximately* 200 *times the magnetic dipole moment from a camouflet explosion. A factor of* 100 *decrease in the initial air density in cavities with radii of* 10 *and* 20 m *results in a reversal of the direction of the magnetic dipole moment vector.*

Key words: *underground nuclear explosion, magnetic dipole moment, decoupling.*

Introduction. The seismic methods included in the international monitoring system are the main means for monitoring underground nuclear explosions (UNE) [1, 2]. A possible method of concealing a UNE is to decrease its seismic performance by conducting the explosion in a cavity of a rather large size (decoupling). The possibility of using decoupling to decrease seismic-wave amplitudes was confirmed by both experiments and numerical modeling [3–8]. Therefore, searching for monitoring methods that would supplement the seismic method is an urgent problem. One of such methods is the recording of magnetic fields during explosions. The fullest experimental data from studies of electric and magnetic fields in UNEs are contained in [9]. A comparison of the magnetic dipole moments produced by camouflet UNEs and explosions of chemical explosives of the same power was made in [10]. Electric and magnetic fields from UNEs in a cavity were analytically estimated in [11]. The present paper reports the results of numerical modeling of magnetic dipole moments produced by UNEs in cavities of various sizes.

Computational Model. The physicomathematical model used in this study is based on the gas-dynamic equations for a one-temperature plasma [12]. We note that the transport coefficients such as viscosity and thermal conductivity are calculated with allowance for the ionic composition, including neutral atoms, whose concentrations are found by solution of the kinetic equations of ionization reactions. Radiation transfer is described in a P1 spectral approximation [13]. The kinetics model uses a radiation-collision approximation, in which the evolution of the plasma ion populations is determined by the following processes: collision ionization, three-particle recombination, photoionization, and photorecombination [14, 15]. For the photoionization and photorecombinations cross sections, quasiclassical Kramers formulas taking into account photoionization from K-shells are used [16]. A complete description of this model is given in [17]. The equation of state for quartz incorporating vaporization is used in the form of [18]. The ionization kinetics equations are solved together with the radiation transfer equation and the equations of gaseous dynamics in one-dimensional spherically symmetric geometry:

$$\frac{d\rho}{dt} = -\frac{\rho}{r^2}\,\frac{\partial}{\partial r}\,(r^2 u),$$

$$\rho\,\frac{du}{dt} = -\frac{\partial}{\partial r}\Big(p + \Pi + \int \frac{U_\nu}{3}\,d\nu\Big),$$

$$\frac{dE}{dt} = -\frac{p+\Pi}{\rho}\,\frac{1}{r^2}\,\frac{\partial}{\partial r}\,(r^2 u) - \frac{1}{r^2}\,\frac{\partial}{\partial r}\,(r^2 q) + Q_{\rm rad},$$

Zababakhin Institute of Technical Physics, Snezhinsk 456770. Translated from Prikladnaya Mekhanika i Tekhnicheskaya Fizika, Vol. 45, No. 3, pp. 3–8, May–June, 2004. Original article submitted March 24, 2003; revision submitted August 15, 2003.

$$\Pi = -\eta\,\frac{1}{r^2}\,\frac{\partial}{\partial r}\,(r^2 u),$$

$$\frac{d}{dt} = \frac{\partial}{\partial t} + u\,\frac{\partial}{\partial r},$$

$$\rho\,\frac{d}{dt}\Big(\frac{U_\nu}{\rho}\Big) + \frac{1}{r^2}\,\frac{\partial}{\partial r}\,(r^2 S_\nu) + \frac{U_\nu}{3r^2}\,\frac{\partial}{\partial r}\,(r^2 u) = Q_\nu - c\chi_\nu U_\nu,$$

$$\frac{\rho}{c}\,\frac{d}{dt}\Big(\frac{S_\nu}{\rho}\Big) + \frac{c}{3}\,\frac{\partial U_\nu}{\partial r} = -\chi_\nu S_\nu,$$

$$\frac{\partial n_i}{\partial t} = \sum n_j W_{ij} - n_i \sum W_{ji}.$$

Here ρ is the density of the material, u is the mass velocity, E is the specific internal energy, c is the speed of light, $q = -æ\nabla T$ is the specific heat flux, $æ$ is the thermal conductivity, T is the temperature, Π is the pressure due to physical viscosity, η is the physical viscosity, S_ν and U_ν are the spectral flux and the radiation energy density, $Q_{\rm rad}$ is the rate of energy transfer between the material and radiation, Q_ν and χ_ν are the source and absorption coefficient of quanta with energy ε_ν, n_i is the population of state i, and W_{ij} is the rate of transition from state j to state i.

The explicit form of the expressions for Q_ν, χ_ν, $æ$, and W_{ij} is contained in [17]. The magnetic dipole moment is calculated as in [11]. In a spherical symmetry approximation, the vector potential $\boldsymbol{A}$ has one component $\boldsymbol{A} = \boldsymbol{e}_\varphi A_\varphi(r,t)\sin\theta$, whose dynamics is described by the equation

$$\frac{d(rA_\varphi)}{dt} = \frac{c^2}{4\pi\sigma}\Big(\frac{\partial^2(rA_\varphi)}{\partial r^2} - \frac{2A_\varphi}{r}\Big) = -\frac{c}{\sigma}\,j_\varphi.$$

The concentrations of ions and neutral atoms are found by numerical solution of the ionization kinetics equations. The conductivity σ is calculated with allowance for the ionic composition of the plasma [19]:

$$\sigma^{-1} = \frac{1}{n_e e^2}\sqrt{\frac{8m_e k_{\rm B} T}{\pi}}\,\Big(\sum_k a_k^{(i)}\sigma_{ek}^{(i)} n_k^{(i)} + \sum_m \sigma_{em}^{(a)} n_m^{(a)}\Big), \qquad \sigma_{ek}^{(i)} = \frac{2\pi\Lambda_{ek} e^4 Z_k^2}{3k_{\rm B}^2 T^2},$$

$$a_k^{(i)} = \frac{0.9073Z_k^4 + 8.4625Z_k^3 + 24.5425Z_k^2 + 22.552Z_k + 5.4168}{3.0752Z_k^4 + 24.208Z_k^3 + 55.816Z_k^2 + 32.128Z_k + 5.4168},$$

where $n_k^{(i)}$ and $n_m^{(a)}$ are the concentrations of ions of type k and neutral species of type m, $\sigma_{ek}^{(i)}$ and $\sigma_{em}^{(a)}$ are the cross sections for elastic dissipation of electrons on ions of type k and neutral species of type m, Z_k is the charge of an ion of type k, Λ_{ek} is a Coulomb logarithm, m_e is the electron weight, e is the elementary charge, $k_{\rm B}$ is Boltzmann's constant, and the coefficients $a_k^{(i)}$ were obtained in [19].

The magnetic dipole moment $\boldsymbol{M}$ is directed along the geomagnetic field and is equal to $\boldsymbol{M} = \dfrac{1}{2c}\displaystyle\int [\boldsymbol{r}\times\boldsymbol{j}]\,dV$. The current density is $\boldsymbol{j} = \boldsymbol{e}_\varphi j_\varphi(r,t)\sin\theta$.

Results of Numerical Modeling. A UNE was modeled by an instantaneous release of an energy of $4.2\cdot 10^{12}$ J (1 kton of TNT equivalent) in an aluminum sphere of 20.7 cm radius. The sphere was in a cavity filled with air. Air was modelled by atomic nitrogen because in the case of small cavity sizes, high temperatures occur ($T > 1$ eV) and, hence, plasmachemical reactions and dissociation energy of molecules can be neglected. Four air densities were considered: a normal density ($\rho = \rho_0 = 1.3\cdot 10^{-3}$ g$\cdot$cm^{-3}) and three lower densities ($\rho/\rho_0 = 10^{-1}$, 10^{-2}, and 10^{-4}). The calculations were performed up to the time of 1 sec for cavity radii of $R = 10$, 20, 80, and 160 m.

Curves of the dipole moment versus time for an explosion in a cavity of 10 m radius in various formulations are shown in Fig. 1. Figures 2 and 3 give r–t diagrams from calculations for this cavity for the normal and lower air densities ($\rho/\rho_0 = 10^{-2}$). For the normal air density, the radiation from the UNE is absorbed in air and no vaporization of the cavity wall occurs. The dipole moment is determined by the motion of the plasma of the explosion products and air in the cavity and reaches the maximum by the moment the shock wave arrives at the cavity boundary (see Fig. 2).

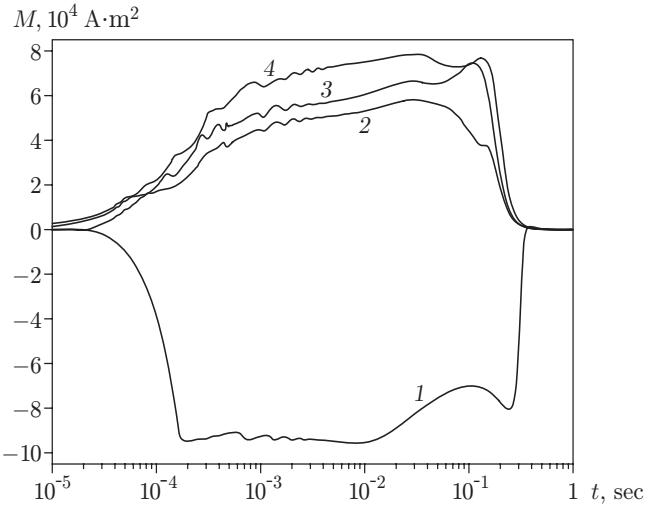

Fig. 1. Magnetic dipole moment versus time in various formulations of the problem for $R = 10$ m: $\rho = 1.3 \cdot 10^{-3}$ (1), $1.3 \cdot 10^{-4}$ (2), $1.3 \cdot 10^{-5}$ (3), and $1.3 \cdot 10^{-7}$ g·cm^{-3} (4).

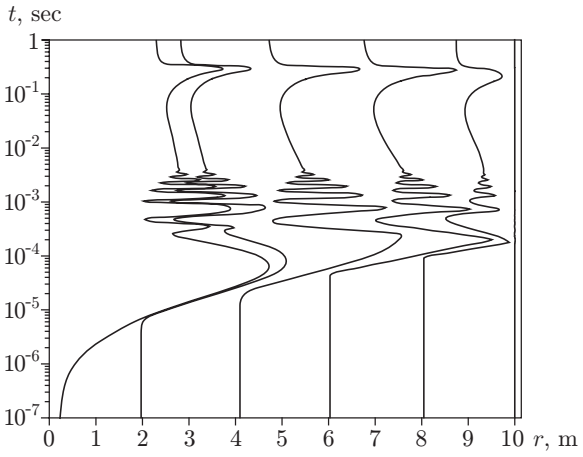

Fig. 2

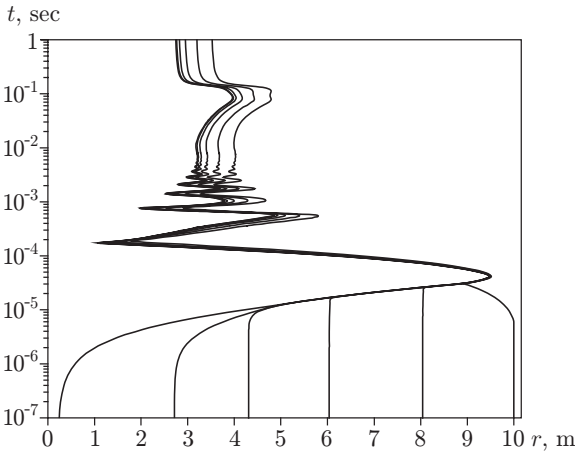

Fig. 3

Fig. 2. r–t diagram for $R = 10$ m and $\rho = 1.3 \cdot 10^{-3}$ g·cm^{-3}.

Fig. 3. r–t diagram for $R = 10$ m and $\rho = 1.3 \cdot 10^{-5}$ g·cm^{-3}.

For the lower air density, the radiation reaches the cavity wall and vaporizes and ionizes it. The motion of the ionized wall material inside the cavity (see Fig. 3) leads to the occurrence of a dipole moment of opposite (than in the previous case) polarity. For an air density of $\rho/\rho_0 = 10^{-1}$, the maximum value of the dipole moment is approximately half the maximum value for the normal density, and a further decrease in air density results in a small increase in the dipole moment. The conductivities of the explosion products and air at various times are shown in Fig. 4.

Curves of the magnetic dipole moment versus time for an explosion in a cavity of 20 m radius are presented in Fig. 5. In comparison with the cavity of 10 m radius, the value of M increases by an order of magnitude due to the larger radius of the sphere from which the geomagnetic field is displaced. The dependence on the initial air density has the same shape as in the previous case. However, unlike in the calculation of the explosion in the cavity of 10 m radius, for $\rho/\rho_0 = 10^{-1}$, the polarity of the dipole moment is negative because the vaporization of the wall is insignificant. The maximum value of M is almost three times smaller than that for the normal air density because of air ionization and the corresponding increase in the conductivity in most of the cavity.

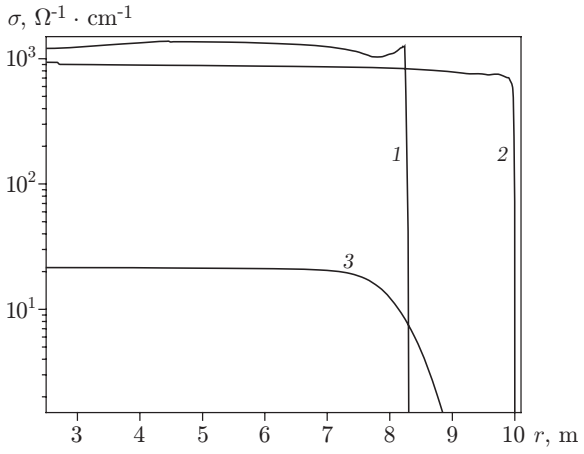

Fig. 4

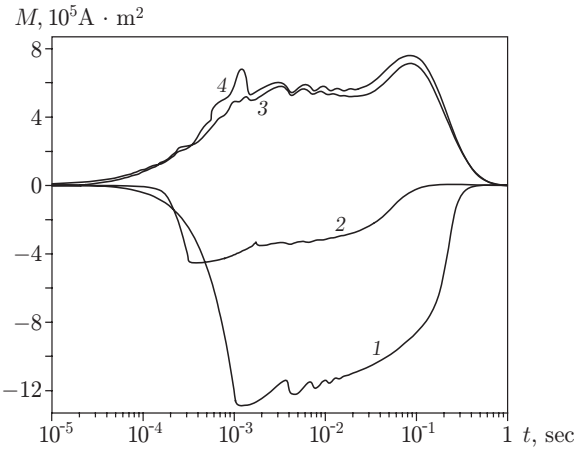

Fig. 5

Fig. 4. Conductivity in the cavity versus time ($R = 10$ m and $\rho = 1.3 \cdot 10^{-3}$ g $\cdot$ cm^{-3}): $t = 10^{-4}$ (1), 10^{-2} (2), and 1 sec (3).

Fig. 5. Magnetic dipole moment versus time in various formulations of the problem for $R = 20$ m: $\rho = 1.3 \cdot 10^{-3}$ (1), $1.3 \cdot 10^{-4}$ (2), $1.3 \cdot 10^{-5}$ (3), $1.3 \cdot 10^{-7}$ g $\cdot$ cm^{-3} (4).

TABLE 1

R, m	M, A $\cdot$ m^2
0	$4.4 \cdot 10^4$
10	$9.5 \cdot 10^4$
20	$1.3 \cdot 10^6$
80	10^7
160	10^7

As the cavity radius increases to 80 m, the signal amplitude increases by another order of magnitude, and with a further increase in the radius, it did not change. The dependence of the amplitude of the magnetic dipole moment on the cavity radius (for the normal air density in the cavity) is given in Table 1.

In the absence of regions with high conductivity outside the cavity, the quasistationary magnetic vector strength $\boldsymbol{H}$ at the measuring point with the radius vector $\boldsymbol{r}$ is found form the magnetic dipole moment vector $\boldsymbol{M}$:

$$\boldsymbol{H} = \frac{3\boldsymbol{r}(\boldsymbol{M} \cdot \boldsymbol{r})}{r^5} - \frac{\boldsymbol{M}}{r^3}.$$

Thus, the magnetic dipole moment changes by a factor of approximately 200, from the values typical of a camouflet UNE, to 10^7 A $\cdot$ m^2 for an explosion in a cavity of large radius. We note that this value corresponds to the effective moment produced by complete displacement of the geomagnetic field from a cavity of radius $R_* \approx 40$ m ($M = 0.5 B_0 R_*^3$, where $B_0 = 0.5$ G is the Earth's magnetic field). A decrease in air density ρ in cavities (of radii 10 and 20 m) from $1.3 \cdot 10^{-3}$ to $1.3 \cdot 10^{-7}$ g $\cdot$ cm^{-3} hardly changes the modulus of the signal amplitude. The change in the signal polarity indicates the presence of a cavity with a lower density.

Conclusions. As follows from the calculation results, a decrease in the seismic signal during decoupling is accompanied by a corresponding increase in the magnetic signal. For example, for a 20 m radius cavity, the decoupling coefficient is 40–110 [8]. In this case, the maximum magnetic dipole moment is 80 times that from a camouflet explosion. Since in a camouflet explosion, magnetic signal variations are easy to detect [9], such measurements can be used as an additional means for monitoring the Comprehensive Nuclear Test Ban Treaty. We note that measurements of the signal shape provide information on the conditions of explosions (presence of a cavity, its size, use of evacuation).

We are grateful to M. I. Avramenko and V. A. Simonenko for fruitful discussions.

This work was supported by the International Scientific and Technical Center (Grant No. KR-214; 2000).

REFERENCES

1. M. Hedlin, "A global test of a time — frequency small-event discriminant," *Bull. Seismol. Soc. Amer.*, **88**, No. 4, 973–988 (1998).
2. V. V. Adushkin and A. A. Spivak, "Wide-scale chemical explosions and the problem of monitoring underground nuclear explosions," in: *Federal Service of Seismological Observations and Earthquake Prediction* [in Russian], Vol. 3, Nos. 1/2 (1996), pp. 107–117.
3. O. Springer, M. Denny, Z. Healy, and W. Mickey, "The Sterling experiment: decoupling of seismic waves by a shot-generated cavity," *J. Geophys. Res.*, **73**, No. 18, 5995–6011 (1968).
4. D. Patterson, "Nuclear decoupling, full and partial," *J. Geophys. Res.*, **71**, No. 14, 3427–3436 (1966).
5. L. A. Glenn and P. Goldstein, "Seismic decoupling with chemical and nuclear explosions in salt," *J. Geophys. Res.*, **99**, No. B6, 11723–11730 (1994).
6. J. L. Stevens, J. R. Murphy, and N. Rimer, "Seismic characteristics of cavity decoupled explosions in salt and tuff," *Bull. Seismol. Soc. Amer.*, **81**, 1272–1291 (1991).
7. V. A. Bychenkov, S. V. Dem'yanovskii, G. V. Kovalenko, et al., "Seismic effectiveness of camouflet underground nuclear explosions," *Vopr. Atomnoi Nauki Tekh.*, Ser. *Teor. Prikl. Fiz.*, No. 2, 22–30 (1992).
8. V. A. Bychenkov, N. S. Zhilyaeva, G. V. Kovalenko, et al., "Possibilities of decreasing and identifying seismic signals from underground nuclear explosions," *Vopr. Atomnoi Nauki Tekh.*, Ser. *Mat. Model. Fiz. Prots.*, No. 3, 18–26 (1996).
9. K. Zablocki, "Electrical transients observed during underground nuclear explosions," *J. Geophys. Res.*, **71**, No. 14, 3523–3542 (1966).
10. G. N. Kovalenko, A. A. Kondrat'ev, Yu. I. Matvienko, et al., "Magnetic dipole moment produced by an explosion of one kiloton of TNT," *Prikl. Mekh. Tech. Fiz.*, **42**, No. 3, 387–392 (2001).
11. L. P. Gorbachev and T. A. Semenova, "Estimation of geomagnetic disturbances due to decoupling," *Atom. Énerg.*, **89**, No. 5, 413–417 (2000).
12. S. I. Braginskii, *Transport Phenomena in Plasma. Problems of Plasma Theory* (collected scientific paper) [in Russian], No. 1, Atomizdat, Moscow (1963).
13. D. Michalas, *Stellar Atmospheres*, Freeman, San Francisco (1978).
14. L. D. Biberman, V. S. Vorob'ev, and I. T. Yakubov, *Kinetics of Nonequilibrium Low-Temperature Plasma* [in Russian], Nauka, Moscow (1982).
15. V. I. Derzhiev, A. G. Zhidkov, and S. I. Yakovlenko, *Ion Radiation in a Nonequilibrium Dense Plasma* [in Russian], Énergoatomizdat, Moscow (1986).
16. I. I. Sobel'man, *Introduction to the Theory of Atomic Spectra* [in Russian], Nauka, Moscow (1977).
17. N. G. Karlykhanov, Yu. V. Martynenko, Yu. I. Matvienko, et al., "Interaction of a plasma flow with a solid-state target," *Fiz. Plasmy*, **22**, No. 11, 998–1006 (1996).
18. A. T. Sapozhnikov and A. V. Pershina, "Interpolation equation of state in the vaporization region," *Vopr. Atomnoi Nauki Tekh.*, No. 2(16), 29–33 (1984).
19. M. A. Erokhin and Yu. I. Matvienko, "Calculation of transfer coefficients in a two-temperature plasma taking into account higher expansion terms," Preprint No. 161, Snezhinsk (1999).